Prompt Photon Production at the Tevatron

Ashish Kumar (for the DØ and CDF collaborations)
Department of Physics, The State University of New York at Buffalo, NY 14260, USA.

DOI: http://dx.doi.org/10.3204/DESY-PROC-2009-03/Kumar

Prompt photon production has been studied by the CDF and DØ experiments at the Fermilab Tevatron collider in $p\bar{p}$ collisions at the centre of mass energy of $\sqrt{s}$ =1.96 TeV. Measurements of the inclusive photon, inclusive photon plus jet, photon plus heavy flavor jet, and diphoton production cross sections are discussed. The analyses use data sample corresponding to integrated luminosity between 0.2 fb^{-1} and 1.02 fb^{-1}. The results are compared to the next to leading order (NLO) perturbative QCD (pQCD) calculations.

1 Introduction

Prompt photon production [1] have been extensively studied both theoretically and by various fixed-target and collider experiments during the last three decades. Prompt photons, sometimes referred to as direct photons, emerge unaltered from the hard interaction between two partons and thus provide a direct probe of the underlying hard-scattering process. Since they emerge without the hadronization phase, they also provide a clean probe without additional complication caused by the parton fragmentation and experimental systematic uncertainties related to jet identification and energy measurement. At the lowest order (LO) in perturbative QCD (pQCD), prompt photons are produced by quark-gluon Compton scattering $gq \rightarrow q\gamma$ and the annihilation subprocess $q\bar{q} \rightarrow g\gamma$. However, the Compton Scattering provides the dominant contribution for photons with moderate transverse momentum (p_T) and the annihilation contribution gains importance at high p_T region. Study of prompt photons, therefore, provide precision tests of our theoretical understanding based on pQCD as well as possible constraint on the relatively poorely measured gluon density of the proton since gluon is involved at tree level in contrast to deep inelastic scattering (DIS) and Drell-Yan (DY) processes where gluon is involved only at a higher order.

Photons in final state may be an important sign of new particles and /or physics beyond the Standard Model. Understanding the QCD production mechanisms of photons is, therefore, a prerequisite to searches for new physics. Prompt photon production cross section measurement is extremely challenging due to enormous background from jets fragmenting into a leading π^0 or η, particularly at low p_T. Photons arising from the decays of π^0 and η are largely suppressed by the photon selection requirements applied to data, and especially by the photon isolation, since these mesons are produced mainly within jets during fragmentation and are surrounded by other particles. Even after very tight selection criteria, highly electromagnetic jets provide a formidable background due to their large cross section. The two showers from the energetic

π^0 or η decaying to two photons coalesce in the calorimeter and mimic single photon shower. Consequently, they can not be rejected on an event-by-event basis and we must perform a statistical background subtraction in order to measure the cross section.

2 Inclusive photon cross section measurement by DØ

DØ has measured the inclusive isolated photon cross section based on an integrated luminosity of 380 pb^{-1} [2]. Central photons ($|\eta|$ <0.9) with p_T > 23 GeV are selected. Photon candidates are formed from clusters of electromagnetic (EM) calorimeter cells within a cone of radius $\mathcal{R} = \sqrt{(\Delta\eta)^2 + (\Delta\phi)^2} = 0.2$ in the space of pseudorapidity (η) and azimuthal angle (ϕ). Candidates are selected if there is significant energy in the EM layers (>95%), and the probability to have a spatially-matched track is less than 0.1%, and they satisfied an isolation requirement. As an isolation criterion, the transverse energy not associated to the photon in a cone of radius $\mathcal{R}$=0.4 around the photon direction has to be less than 0.10 times the energy of the photon. Potential backgrounds from cosmic rays and electrons from W boson decays are suppressed by requiring the missing transverse energy (E_T^{miss}) to be less than 0.7 p_T. To better select photons and estimate the residual background, an artificial neural network ($\gamma - ANN$) is constructed using the powerful discriminating variables exploiting information from the calorimeter and the tracker. The $\gamma - ANN$ was trained to discriminate between direct photons and background events. The photon purity ($\mathcal{P}$) is determined statistically for each photon p_T bin by fitting the $\gamma - ANN$ distribution in data to predicted $\gamma - ANN$ distributions for signal and background Monte Carlo (MC) samples.

The measured cross section, together with statistical and systematic uncertainties, is presented in Fig.1 and compared with the results from a next-to-leading order (NLO) pQCD calculation obtained from JETPHOX program [3] . These results were derived using the CTEQ6.1M parton distributions functions (PDFs) and the BFG fragmentation functions (FFs). The renormalization, factorization, and fragmentation scales were chosen to be equal to photon p_T. The ratio of the measured to predicted cross sections is also shown in Fig.1. The scale dependence, estimated by varying scales by factors of two, are displayed as dashed lines. As can be seen, the results are consistent with theory within uncertainties. The difference in shape between data and theory at low p_T is difficult to interpret due to the large theoretical and experimental uncertainties. Higher order calculations are expected to reduce the scale sensitivity and calculations that account for soft-gluon contributions are expected to provide better descriptions of the data at low p_T.

3 Inclusive photon cross section measurement by CDF

CDF has recently presented a preliminary result on the measurement of the inclusive isolated photon cross section using a data set corresponding to an integrated luminosity of 2.5 fb^{-1} [4]. Measurements are performed as a function of the photon p_T for photons with p_T >30 GeV and $|\eta|$ <1.0. Photon candidates are required to be isolated in the calorimeter with E_T^{iso} >2.0 GeV, where E_T^{iso} is defined as the transverse energy deposited in a cone of radius $\mathcal{R}$=0.4 around the photon candidate minus that of the photon. To reject electrons from W decays and non-collision backgrounds, candidates with $E_T^{miss} > 0.8 p_T$ are vetoed. The calorimeter isolation distribution

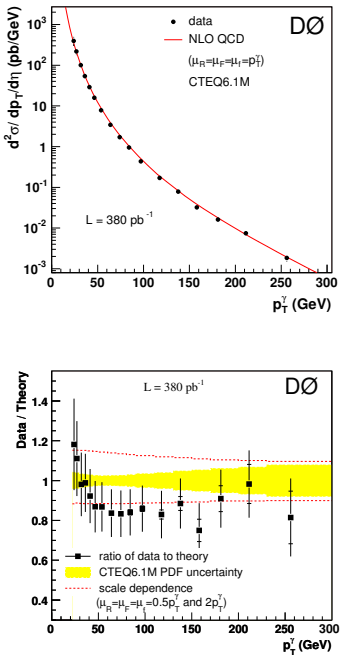

Figure 1: The measured differential cross section for isolated photon production by DØ (Top) and the ratio of measured to predicted cross section by JETPHOX (Bottom).

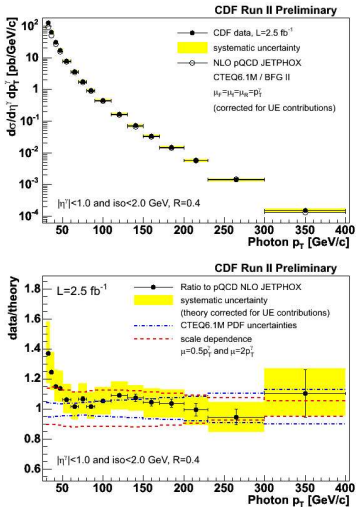

Figure 2: The inclusive isolated photon cross section as a function of the photon transverse momentum measured by the CDF experiment (Top). The p_T spectrum of the ratio of measured to NLO calculations is shown (Bottom).

is employed to discriminate photon signal from QCD background (dominated by π^0 decays). Templates for signal and background are constructed using Monte Carlo simulations and fitted to the data in each bin of p_T to estimate the photon purity in the selected sample. The obtained photon signal fraction varies from 70% to 100% as the photon p_T increases.

The p_T distribution of the measured cross section is unfolded back to the parton level for comparison with the theory. The unfolding factors, which takes into account both the efficiencies, detector resolution effects and acceptance effects, vary between 64% to 69% in the p_T range considered. The systematic uncertainties in the cross section range from 10% to 15%, dominated by the photon purity determination at low p_T and by the uncertainty in the photon energy scale at high p_T. The cross section is measured as a function of the photon p_T up to 400 GeV and compared to the NLO pQCD predictions as given by the JETPHOX program [3], with CTEQ6.1M PDFs and BFGII fragmentation functions. Figure 2 shows these results that test the pQCD over 6 orders of magnitude. The renormalization, factorization and fragmentation scales are all set to the photon p_T. The theory is corrected for the non-perturbative effects from the underlying event and this correction decreases the theoretical cross section by approximately 9%, and is independent of p_T. The ratio of the measured and predicted cross sections as a function of the photon p_T is also presented in Fig. 2. Theory and data agree well over the whole measured range except for $p_T < 40$ GeV. For p$p_T < 40$ GeV the data exhibits an excess and a different shape, consistent with similar observation in previous measurements.

4 Inclusive photon + jet cross section by DØ

The production of a photon with associated jets in the final state is more sensitive to the underlying dynamics of hard QCD interactions than the inclusive photon measurements. DØ has measured the inclusive differential cross section of photon plus jet production based on an integrated luminosity of 1.0 fb^{-1} [5]. The study considers different angular configurations between the photon and the jets to probe different regions of parton momentum fraction x and hard-scattering scales Q^2. Photons with $p_T > 30$ GeV and central rapidity $|\eta|$ <1.0 are considered in the analysis. Photon candidates are required to deposit at least 96% of the detected energy in the EM calorimeter layers and should not be spatially matched to a reconstructed track. The isolation criteria requires the transverse energy not associated to the photon in a cone of radius $\mathcal{R}$=0.4 around the photon direction to be less than 0.07 times the energy of the photon. Backgrounds from cosmics and electrons from W boson decays are vetoed by a missing transverse energy requirement of $E_T^{miss} < (12.5 + 0.36p_T)$ GeV. Electromagnetic cluster and track information is fed into a neural network to further increase the photon purity. Jets are reconstructed with a midpoint cone algorithm with $\mathcal{R}$=0.7. Events containing at least one jet are selected which must have p_T >15 GeV and can be either central (y^{jet} <0.8) or forward (1.5< y^{jet} <2.5). Finally, the photon candidate and the leading hadronic jet are required to be separated in η-ϕ phase space by > 0.7. The photon purity of the sample in different p_T bins is determined by fitting the MC templates of $\gamma - ANN$ in data.

The measured triple differential cross sections measured are shown in Fig. 3 as a function of photon p_T with the full experimental (systematic $\oplus$ statistical) errors for different kinematic regions (distinguished by central and forward jets and same-side and opposite-side photon and

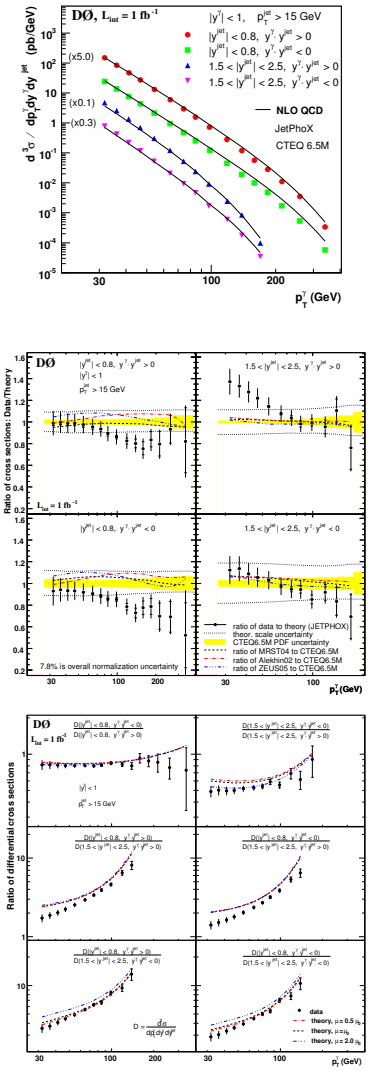

Figure 3: The differential photon + jet cross section as a function of the photon p_T in four different kinematic regions (Top), the corresponding data/theory ratio (Middle) and the ratios between the differential cross sections in each y^{jet} region.

jet rapidities). These four kinematic regions probe different momentum phase space of the two initial interacting partons. The largest uncertainties are caused by the purity estimation, photon and jet selections and luminosity. Statistical errors vary from 0.1% in the first p_T bin to $13-20\%$ in the last bin, while systematic errors are within $10-15\%$ depending on the region. The superimposed theoretical curve corresponds to the NLO QCD predictions based on the JETPHOX program [3] with the CTEQ6.5M set of PDFs and BFG set of fragmentation functions. The choice of renormalization (μ_R), factorization (μ_F) and fragmentation (μ_f) scales used is $\mu_R = \mu_F = \mu_f = p_T^\gamma f(y^\star)$ with $f(y^\star) = ([1+exp(-2|y^\star|)]/2)^{1/2}$ and $y^\star = 0.5(\eta^\gamma - \eta^{jet})$. Non-pQCD effects were considered to be negligible. The ratio of the measured cross sections to the NLO predictions are presented in Fig.3 for the different regions. As shown in Fig. 3, the predictions do not describe the shape of the data for the whole measured range, especially for jet y^{jet} <0.8 and p_T > 100 GeV and for 1.5< y^{jet} <2.5, $y^\gamma.y^{jet}$ >0 and p_T <50 GeV, where the difference in shapes is similar to those observed in previous inclusive photon measurements. Figure 3 also shows the ratio of measured cross sections in the different regions where the experimental systematic uncertainties are reduced further. In general, the shapes of the measured cross section ratios in data are qualitatively reproduced by the theory but a quantitative disagreement is observed for some kinematic regions even after taking into account the overall (experimental and theoretical) uncertainty.

5 Inclusive photon + heavy flavor jet cross section by DØ

DØ has performed the first measurements of the differential cross section of the inclusive photon production in association with heavy flavor (b and c) jets at a $p\bar{p}$ collider using 1.02 fb^{-1} of data [6]. The analysis considers one isolated photon with $p_T > 30$ GeV in the central rapidity region of $|\eta|$ <1.0. Photons are essentially subjected to the same selection as in Section 4. Background from dijet events containing π^0 and η mesons is suppressed using an artificial neural network ($\gamma - ANN$). Backgrounds from cosmics and electrons from W boson decays are vetoed by a missing transverse energy requirement of $E_T^{miss} < 0.7p_T$. Jets are reconstructed with a midpoint cone algorithm with radius of $\mathcal{R} = 0.5$. and are required to have $p_T > 15$ GeV and y^{jet} <0.8. Same side and opposite side photon and jet rapidity events are treated separately. The leading jet must have at least two tracks associated with hits in the silicon microstrip tracker for the heavy flavor tagging. A dedicated neural network ($b - ANN$) which exploits the longer lifetimes of heavy flavored hadrons is applied to enrich the heavy flavor jet content of the considered events. The $b - ANN$ selection has an efficiency of 55-62% for b jets and of 11-12% for c jets. Only 0.2-1% of light jets are misidentified as heavy-flavor jets. Photon purity is estimated in each p_T bin using the $\gamma - ANN$ distribution. The fractional contributions of b and c jets are determined by fitting templates of $P_{\text{HF-jet}} = -\ln\prod_i \text{Prob}^i_{\text{track}}$ (Fig. 4) to the data, where $\text{Prob}^i_{\text{track}}$ is the probability that a track originates from the primary vertex. The templates for b and c jets are obtained from MC, and the light jet templates come from a data sample enriched with light jets. Jets from heavy quarks have typically large values of $P_{\text{HF-jet}}$. The estimated fractions of b and c jets in the p_T bins vary between 25-34% and 40-48% respectively.

The measured differential cross sections are shown in Fig. 4 for $\gamma + b + X$ and $\gamma + c + X$ production as a function of photon p_T for two different kinematical regions defined by $y^\gamma y^{jet}$ >0 and $y^\gamma y^{jet}$ <0. The cross section falls by more than three orders of magnitude in the range

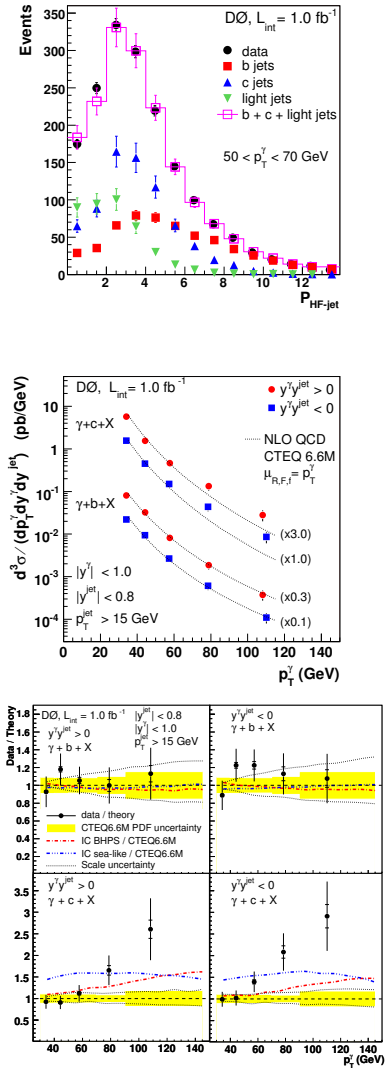

Figure 4: Distributions of observed events for P_{HF-jet} for photon p_T 50< p_T <70 GeV. The distributions for the b,c and light jet templates are also shown (Top). The $\gamma + b + X$ and $\gamma + c + X$ differential cross sections as a function of photon p_T in the two regions $y^{\gamma}y^{jet}$ >0 and $y^{\gamma}y^{jet}$ <0 (Middle). the data-to-theory ratio of cross sections for $\gamma + b + X$ and $\gamma + c + X$ in the corresponding regions (Bottom).

$30 < p_T < 150$ GeV. The statistical uncertainty on the results ranges from 2% in the first p_T bin to 9% in the last bin, while the total systematic uncertainty varies between 15% and 28%. The uncertainty at low p_T is mainly due to the photon purity, while at higher p_T, it is dominated by the heavy flavor fraction. The result is compared to the NLO pQCD predictions [7] with CTEQ6.6M PDFs and all the theory scales set to photon p_T ($\mu_R = \mu_F = \mu_f = p_T$). The predictions have been corrected for parton-to-hadron fragmentation effects by 7.5% (3%) in the b (c) jet cross section for low p_T and by 1% at high p_T. The ratio of the measured to predicted cross sections are also shown in Fig. 4. While the prediction agrees with the measured cross section for $\gamma + b + X$ production over the entire p_T range, the prediction underestimates the measured cross section for $\gamma+c+X$ production for p_T above 70 GeV. The measurements are also compared to predictions including two models with intrinsic charm parameterizations in the CTEQ6.6M PDF. Both non-perturbative models predict a higher $\gamma+c+X$, but, do not describe the measured cross section. The observed difference in the shape could be due to an underestimation of the $g \to Q\bar{Q}$ splitting in the annihilation process which becomes dominant at high p_T.

6 Inclusive diphoton cross section measurement by CDF

The measurements of prompt diphoton production provide a great test of QCD production mechanisms and they are also possible signatures of "new" physics. The diphoton anaysis allows a direct measurement of the transverse momentum of the $\gamma\gamma$ system (q_T) which is sensitive to initial-state soft gluon radiation. It is also one of the important backgrounds for Higgs $\to \gamma\gamma$ searches at the LHC. CDF has measured the inclusive diphoton cross section using a data sample of 207 pb^{-1} [8]. The leading contributions to the diphoton production arise from quark-antiquark annihilation and from gluon-gluon scattering. In addition to the prompt production, the diphoton cross section also receives contribution where one or both photons are produced in fragmentation processes which are largely suppressed by photon isolation. Central photon candidates ($|\eta|$ <0.9) with transverse energy (E_T) greater than 14 GeV (13 GeV) for the leading (softer) photons are selected based on lateral shower profile, preshower hit and no associated track requirements. The isolation requirement requires the transverse energy in a cone of radius R=0.4 around the photon direction, not associated with the photon, to be below 1 GeV. In total 427±59 (stat) diphoton events in 889 diphoton candidates are selected in the analysis.

Figure 5 shows the differential diphoton cross section as a function of invariant diphoton mass ($M_{\gamma\gamma}$), q_T , and the difference in azimuthal angle between two photons ($\Delta\phi_{\gamma\gamma}$). The results are compared to the theoretical predictions of DIPHOX [9], ResBos [10] and Pythia [11]. DIPHOX includes NLO matrix elements for both the direct contribution and the fragmentation contribution and the NNLO contribution from $gg \to \gamma\gamma$. ResBos includes the fragmentation contributions only at LO but it implements the resummation of soft initial-state gluon radiation which is relevant at low q_T. Also shown are the results for PYTHIA (LO matrix elements for both the direct and fragmentation contribution) which has been scaled by a factor of 2 to match the data. The contributions from fragmentation processes are especially large in regions of small $M_{\gamma\gamma}$, large q_T and small $\Delta\phi_{\gamma\gamma}$ and these regions are only described by DIPHOX which includes the NLO corrections for the fragmentation process. The kinematic regions at low q_T and large $\Delta\phi_{\gamma\gamma}$ are especially sensitive to soft initial-state gluon emissions and ResBos describes

this phase space, thanks to the resummation effects it incorporates. Describing the diphoton production in all regions of phase space simultaneously requires a full NLO calculation taking higher order $gg \rightarrow \gamma\gamma$ corrections and resummed soft-gluon radiation into account.

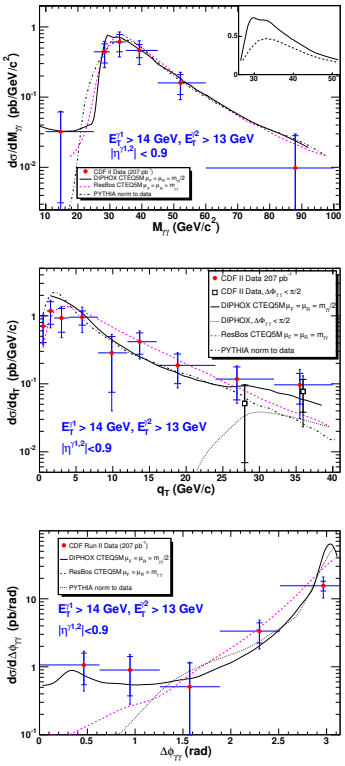

Figure 5: The differential diphoton cross section as a function of invariant diphoton mass ($M_{\gamma\gamma}$), transverse momentum of the diphoton system q_T , and the difference in azimuthal angle between two photons ($\Delta\phi_{\gamma\gamma}$) along with the predictions from DIPHOX, ResBos and Pythia.

7 Conclusions

Incluisve isolated photon, photon plus jet, diphoton and photon plus heavy flavor jet cross sections have been measured by the CDF and DØ experiments in $p\bar{p}$ collisions at the Fermilab Tevatron. Inclusive isolated photon cross section measurements show a different shape at low photon p_T consistent with observation in previous measurements by UA2, CDF and DØ . The differential photon plus jet cross section has been measured in four distinct kinematic regions resulting in similar shapes as in the inclusive photon measurement. The theory can not describe the measurement in the whole measured range, especially for y^{jet} <0.8 and $p_T > 100$ GeV and for 1.5< y^{jet} <2.5, $y^{\gamma}.y^{jet}$ >0 and p_T < 50 GeV. First measurements on $\gamma + b + X$ and $\gamma + c + X$ cross sections have been presented. Good agreement with theory is observed in case of b jets, while theory underestimates the measured $\gamma + c + X$ cross section for p_T >70

GeV. The differential diphoton production cross section has been measured as a function of diphoton invariant mass, transverse momentum and azimuthal opening angle and compared to the theoretical calculations. These quantities can not be described simultaneously by a single theoretical model.

References

[1] J.F. Owens, Rev. Mod. Phys. **59** 465 (1987).

[2] V. Abazov *et al.* (DØ collaboration), Phys. Lett. B**639** 151 (2006).

[3] S. Catani, F. Fontannaz,J.P. Guillet and E. Pilon, JHEP **05** 028 (2002).

[4] C. Deluca (CDF collaboration), arXiv:hep-ex/09052201 (2009).

[5] V. Abazov *et al.* (DØ collaboration), Phys. Lett. B**666** 435 (2008).

[6] V. Abazov *et al.* (DØ collaboration), accepted for publication in Phys. Rev. Lett., FERMILAB-PUB-**08-582-E**.

[7] T. Stavrera and J. Owens, Phys. Rev. D**79** 054017 (2009).

[8] D. Acosta *et al.* (CDF collaboration), Phys. Rev. Lett. **95** 022003 (2005).

[9] T. Binoth, J.P. Guillet, E. Pilon and M. Werlen, Eur. Phys. J. **C16** 311 (2000).

[10] C. Balazs, E.L. Berger, S. Mrenna and C.P. Yuan, Phys. Rev. D**57** 6934 (1998)

[11] T. Sjostrand *et al.*, Comp. Phys. Comm. **135** 238 (2001).